How does ultrasonic cavitation remove dental bacterial biofilm?

Vyas, N.; Wang, Qian; Manmi, K.a.; Sammons, R.l.; Kuehne, S.a.; Walmsley, A.d.

DOI:
10.1016/j.ultsonch.2020.105112

License:
Other (please provide link to licence statement

Document Version
Publisher's PDF, also known as Version of record

Citation for published version (Harvard):
Vyas, N, Wang, Q, Manmi, KA, Sammons, RL, Kuehne, SA & Walmsley, AD 2020, 'How does ultrasonic cavitation remove dental bacterial biofilm?', *Ultrasonics Sonochemistry*, vol. 67, 105112. https://doi.org/10.1016/j.ultsonch.2020.105112

Ultrasonics - Sonochemistry 67 (2020) 105112

Contents lists available at ScienceDirect

Ultrasonics - Sonochemistry

journal homepage: www.elsevier.com/locate/ultson

How does ultrasonic cavitation remove dental bacterial biofilm?

N. Vyas[a], Q.X. Wang[b], K.A. Manmi[b,c], R.L. Sammons[a], S.A. Kuehne[a], A.D. Walmsley[a,*]

[a] School of Dentistry, College of Medical and Dental Sciences, University of Birmingham, 5 Mill Pool Way, Birmingham B5 7EG, UK
[b] School of Mathematics, University of Birmingham, Edgbaston, Birmingham B15 2TT, UK
[c] Department of Mathematics, College of Science, Salahaddin University-Erbil, Kurdistan Region, Iraq

A B S T R A C T

Bacterial biofilm accumulation is problematic in many areas, leading to biofouling in the marine environment and the food industry, and infections in healthcare. Physical disruption of biofilms has become an important area of research. In dentistry, biofilm removal is essential to maintain health. The aim of this study is to observe biofilm disruption due to cavitation generated by a dental ultrasonic scaler (P5XS, Acteon) using a high speed camera and determine how this is achieved. *Streptococcus sanguinis* biofilm was grown on Thermanox™ coverslips (Nunc, USA) for 4 days. After fixing and staining with crystal violet, biofilm removal was imaged using a high speed camera (AX200, Photron). An ultrasonic scaler tip (tip 10P) was held 2 mm away from the biofilm and operated for 2 s. Bubble oscillations were observed from high speed image sequences and image analysis was used to track bubble motion and calculate changes in bubble radius and velocity on the surface. The results demonstrate that most of the biofilm disruption occurs through cavitation bubbles contacting the surface within 2 s, whether individually or in cavitation clouds. Cleaning occurs through shape oscillating microbubbles on the surface as well as through fluid flow.

1. Introduction

Biofilm removal by ultrasound through the generation of cavitation bubbles is a developing area of research in healthcare. Cavitation is the formation and rapid collapse of gas or vapour bubbles in a liquid that may occur when ultrasound is applied [1]. The forces generated from cavitation bubbles and acoustic streaming (fluid flow) are applied to a wide range of industries including removing biofouling in marine environments, decontamination in the food industry, semiconductor cleaning and removal of bacterial biofilm in medical and dental applications [2–7]. Biofilm infections in healthcare are a particular problem as they cannot be effectively treated with antibiotics due to the increase in antimicrobial resistance [8]. Therefore physical removal is an increasing research area for disruption of attached microbial plaques [9]. Cavitation has the potential to clean biofilms from a substrate at the microscopic level with minimal damage to the underlying surface. A challenge in using cavitation effectively for this process is that the exact cavitation phenomena occurring during disruption have not yet been elucidated [5,10]. There are many factors which influence the removal ability of cavitation from ultrasonic scalers and it is unpredictable, which is a major challenge for optimising it for different cleaning applications. To make efficient use of it the exact mechanisms underlying the cleaning processes require identification so they can be optimized [11]. Cleaning takes place via several mechanisms including microjets formed during bubble collapse creating localised shear forces on the surrounding biofilm [5,12], cavitation cloud collapse [13], shock waves released during bubble implosion, microstreamers, acoustic streaming in the bulk fluid and microstreaming around individual cavitation bubbles as they oscillate [10]. Whilst biofilm removal via cavitation has been studied previously using high speed imaging [14], the slower shutter speeds that were used gave blurred outlines of the bubble motion and the exact bubble dynamics could not be elucidated.

The aim of this study was to provide a protocol for biofilm removal imaging using a high speed camera. The use of high speed imaging provides information about the biofilm removal process using ultrasonic cavitation. This will then allow the ultrasonic generators to be optimised for different biofilm removal applications. Cavitation for root canal cleaning has been studied previously [14–17] but there are limited studies on the use of ultrasonic scalers, which clean dental plaque from the outer surfaces of teeth and dental implants. A current clinical challenge with dental ultrasonic scalers is the removal of biofilm from the surface of titanium dental implants. As the use of this treatment method increases, the care and maintenance of the implant is pivotal to their long term success. Current methods used for biofilm removal from dental implants either damage the titanium implant surface, which further exacerbates the biofilm formation due to increased surface roughness [18,19], or they cannot fully remove the biofilm. Dental implants have several features such as a rough surface or a screw based design [20]. These help increase surface area of the implant surface allowing improved integration with the surrounding bone. If these surfaces become exposed then they are not amenable to cleaning with traditional instrumentation. It can be argued that whilst the metal

* Corresponding author.
E-mail address: a.d.walmsley@bham.ac.uk (A.D. Walmsley).

https://doi.org/10.1016/j.ultsonch.2020.105112
Received 2 September 2019; Received in revised form 4 February 2020; Accepted 26 March 2020
Available online 28 March 2020

impact from ultrasonic scalers may damage dental implants, the cavitation occurring in the cooling water flowing around the ultrasonic scaler tips will still remove biofilm and be used as a novel method of cleaning. Also, the use of cavitation will allow the scaler to be held away from the surface for effective cleaning.

In this study we use high speed imaging and image analysis to image cavitation bubbles from an ultrasonic scaler disrupting biofilm on a coverslip. We demonstrate that cleaning occurs through shape oscillating microbubbles on the surface as well as through fluid flow.

2. Materials and methods

2.1. Biofilm growth

The Gram-positive bacteria *Streptococcus sanguinis* (ATCC 10556) was used in the current study to form a simplistic early biofilm model for understanding the cavitation phenomena. Briefly, the stock microorganisms were recovered from porous storage beads maintained at −80 °C and initially grown on Tryptone Soya Agar (Oxoid, UK) media at 37 °C with 5% CO_2 for 3 days. Two to three single colonies were used to inoculate 10 ml of Brain Heart Infusion (BHI) medium (Oxoid, U.K.) supplemented with 1% sucrose (Fluka Analytical, UK), which was incubated at 37 °C, shaking at 88 rpm overnight until it reached approximately 10^9 colony forming units/ml. This primary culture was serially diluted to 10^3 cfu/ml in BHI medium.

Artificial saliva was added to the biofilm culture surface to promote biofilm formation, this was prepared according to the method described by Pratten et al. [21], with the following chemicals from Sigma, UK (unless stated otherwise) added sequentially to RO (reverse osmosis) water: 0.35 g/L sodium chloride (NaCl), 0.2 g/L potassium chloride (KCL), 0.2 g/L calcium chloride (CaCl2), 2 g/L yeast extract, 1 g/L lab lemco powder, 2.5 g/L hog gastric mucin and 5 g/L proteose peptone. Reagents were mixed on a magnetic stir plate (Fisher scientific, Loughborough, UK) at ambient temperature for 1 h. After autoclaving 1.25 ml of 40% sterile filtered urea (0.22 μm filter) was added to 1 L of the prepared artificial saliva. The prepared media was wrapped with aluminium foil to exclude light and prevent protein degradation [22] before being stored at 4 ± 1 °C. 1 ml of the artificial saliva was pipetted into each well of a 24-well plate into which a sterile Thermanox™ coverslip (13 mm, Nunc, ThermoFisher Scientific) had been placed and was removed after 15 min, to condition the samples. One side of the coverslips was bent upwards using sterile forceps to create a lip so the samples could be removed from the well with minimal biofilm disruption. The Thermanox™ coverslips have a smooth, homogenous surface with a surface roughness of 0.02 ± 0.001 μm as measured by surface profilometry.

One ml of the diluted *S. sanguinis* culture and 1 ml of fresh BHI medium was added to each well of the 24-well plates. The 24-well plates were then incubated at 37 °C, 88 rpm for 24 h to allow biofilm formation. The broth was replaced with 2 ml fresh BHI medium every 24 h. The Thermanox™ coverslips were removed from the 24 well plates after a total of 4 days of incubation and then fixed in 0.1 M sodium cacodylate buffer and 2.5% glutaraldehyde (25% EM grade, Agar Scientific, Essex, UK). They were then stained with Crystal Violet stain (Pro-Lab Diagnostics, UK) for 5 min and gently washed in Phosphate Buffered Saline (PBS) (Sigma-Aldrich, USA). Samples were stored in PBS until high speed imaging to prevent dehydration.

2.2. High speed imaging

Biofilm removal using cavitation from an ultrasonic scaler tip was imaged using a high speed camera (Fig. 1). The coverslip with biofilm was fixed vertically in a custom-made glass water tank with dimensions 2.7 cm × 2.7 cm × 2.7 cm. The tank was filled with 15 ml reverse osmosis (RO) water. A P5 Newtron XS scaler (Satelec, Acteon, France) was used in conjunction with Tip 10P. The tip was immersed in the glass water tank and its position was fixed by attaching it to a XYZ translation stage (PT3, Thorlabs Inc, NJ, USA) and a high-precision rotation mount (PRO1/M, Thorlabs Inc, NJ, USA). The axial rotation of the scaler tip was also maintained during each experiment. The sample was illuminated using an LED cold light source (Hayashi HDF7010, Japan) in bright field mode. The biofilm removal was imaged using a high speed camera (Fastcam mini AX200, Photron, Japan). A long distance microscope zoom lens was attached to the camera (12 × x zoom lens system, Navitar, USA) with a 2x adapter, giving a working distance of 32 mm. The scaler tip was operated at medium power (power 10) for 2 s, 2 mm away from the biofilm. It is difficult to measure the power output from the tip due to its shape. The energy also radiates outwards. The best method is to cite the tip vibration for comparison with other studies. At this power setting the displacement of the free end of the tip is 80 μm [23]. High speed imaging was done at 2000 frames per second (fps) or 10 k fps, with a shutter speed of 1/300,000 s and a magnification of x7, giving a resolution of 1.429 μm/pixel or x2, giving a resolution of 5 μm/pixel.

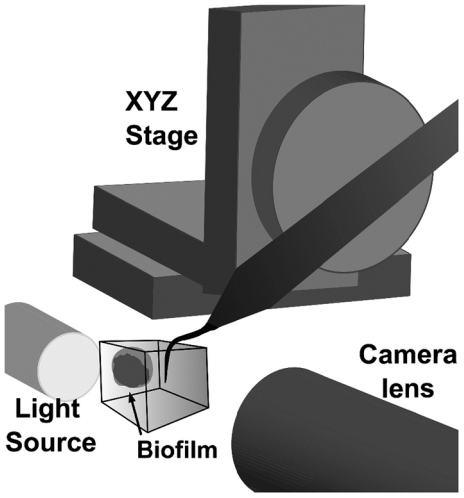

Fig. 1. Schematic of the experimental setup for high speed imaging of biofilm removal, showing the ultrasonic scaler hand piece fixed to an XYZ translation stage. The tip was immersed in a water tank in which the biofilm was fixed vertically, allowing for high speed imaging in bright field mode.

2.3. Image analysis

Image analysis was done using Fiji (ImageJ, U.S. National Institutes of Health, Bethesda, Maryland, USA) [24]. Tracking was done using the Trackmate plugin [25]. Two bubbles were manually tracked in each video, and 5 videos were analysed, resulting in 10 tracks (supplementary video a). The bubble radius and speed on the surface at intervals of 0.02 s were calculated from high speed videos taken at 2000 fps with 5 μm pixel size. Data analysis and graphing were done using Sigmaplot Version 13.0.

Contrast was enhanced in some high speed videos using the gamma non-linear histogram adjustment to differentiate between the opaque biofilm clusters and the more translucent biofilm.

3. Results and discussion

3.1. High speed imaging observations

High speed imaging showed that biofilm was removed radially away from the scaler, starting from the area closest to the scaler tip (Fig. 2, supplementary video a).

Most of the biofilm in the field of view was removed within the 2 s operation of the scaler. In clinical use the tip of the ultrasonic scaler is moved constantly. If the ultrasonic scaler is used in a non-touch mode

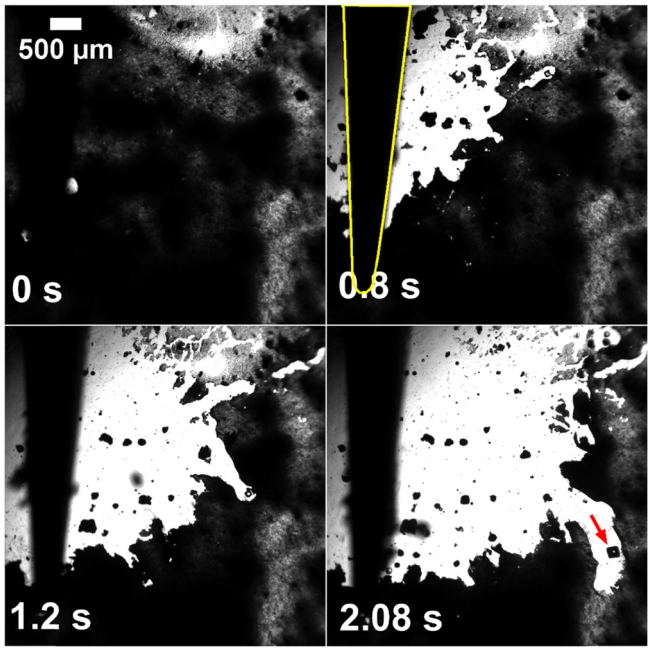

Fig. 2. High speed image stills showing biofilm being removed via cavitation from an ultrasonic scaler tip (outlined in yellow in the second image) immersed in water. Most biofilm within the vicinity of the tip is removed within 2 s (white area is where the biofilm has been removed). Bubbles can be seen on the coverslip surface removing biofilm as they travel across the surface away from the scaler tip. Bubbles on the surface showed shape oscillations, for example a bubble is in square shape mode 4 (red arrow). Also see supplementary video a, which shows the high speed video along with lines showing the direction of some of the bubbles. (For interpretation of the references to colour in this figure legend, the reader is referred to the web version of this article.)

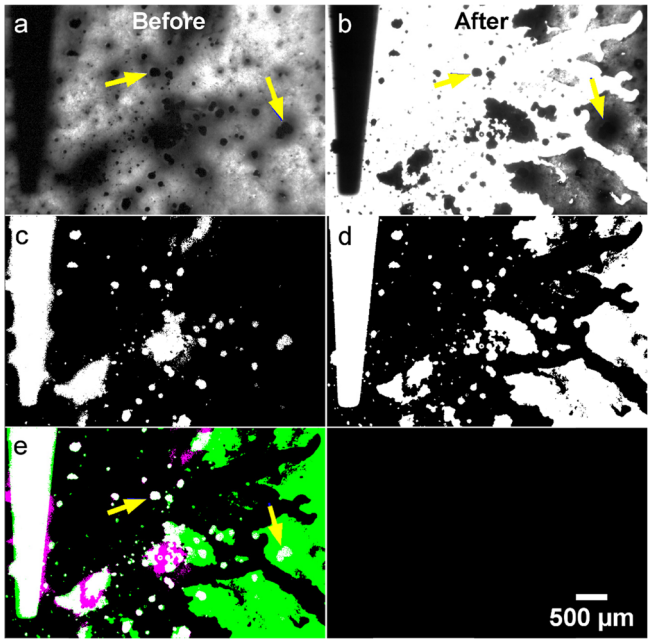

Fig. 3. Biofilm clusters (some labelled with yellow arrows) which were more opaque were not removed by the cavitation bubbles at the setting investigated. (a) High speed image taken before biofilm removal, contrast enhanced using the gamma adjustment. The ultrasonic scaler tip is in the left of the image (b) After the ultrasonic scaler was operated for 2 s (c) Binary thresholded image of (a) to keep only the opaque areas of biofilm (d) Binary thresholded image of d (e) Overlay of the before and after thresholded images, where the pink areas show pixels present in the image before biofilm removal but not after, the green areas show pixels present in the image after biofilm removal but not before, and the white areas show pixels overlapping in the before and after images. The opaque biofilm clusters present before are also present after biofilm removal, showing that they were not removed. Cavitation bubbles moving on the surface have made paths around these clusters. (For interpretation of the references to colour in this figure legend, the reader is referred to the web version of this article.)

for cleaning with cavitation in the future, these results suggest that it could be held for 2 s at each location around a tooth or dental implant.

There were however some parts of the biofilm which were not removed in the 2 s time period. These could also not be removed after 20 s of applying the scaler at the same power and distance. The high speed images show that these structures, which for the purposes of this discussion are termed “biofilm clusters”, are more opaque than the rest of the attached structure. Fig. 3 demonstrates that the opaque biofilm clusters observed before biofilm removal are the same as those which are still attached to the surface after the disruption. High speed videos also show that if the bubbles encountered a biofilm cluster, they would either change course or oscillate next to the cluster without being able to disrupt it (supplementary video b). They eventually changed direction to continue moving across the surface. We speculate that these biofilm clusters have a larger adhesive force to the surface. Rivas et al. also imaged biofilm removal using cavitation, and their images show that the biofilm they used also had different opacities, but they do not show a difference in biofilm removal [14]. Rivas et al. have measured the adhesion of 20 µm thick biofilm using a hydrodynamic technique to be of the order of 10^{-1}N/m^2. However they used a different biofilm species (*Pseudomonas aeruginosa* and *Enterococcus faecalis*), which may have different attachment properties to the *S. sanguinis* biofilm used in the current study. It is unlikely that the cavitation in the current study was not vigorous enough to achieve proper removal because other parts of the biofilm were removed readily, therefore it is likely that the disruption was different due to changes in biofilm structure. The clusters observed in the current study may be the initial attachment points when the biofilm started to form or they may be formed of a denser population of bacteria with a different amount of extracellular polymeric matrix present. The surface is homogeneous and smooth, therefore the clusters are not formed due to changes in the roughness of the surface. Further research is required to understand if these clusters form in other biofilm species, how they are affected by surface roughness and whether they have different attachment forces to the surrounding biofilm.

Cleaning effects are associated with both individual bubbles and clouds of bubbles. One main finding in this study is cavitation clouds impacting on the biofilm caused an immediate larger scale disruption of biofilm (Fig. 4). Previous work showed that cavitation clouds can detach from the tip and be propelled into the water [23]. Although in most cases the cavitation clouds originating around the tip of the ultrasonic scaler did not reach the surface because it was 2 mm away, in one high speed video (Fig. 5) a bubble cloud grew and then impacted the biofilm (Supplementary video c), causing disruption. If the ultrasonic scaler tip is held closer to the surface (approximately 0.5 mm away), then quicker biofilm disruption from the cavitation clouds could occur. This may also be able to remove parts of the biofilm which have higher attachment forces to the surface.

Another main finding is that an individual bubble in shape oscillation, translating in contact with the biofilm, cleans the biofilm rapidly along its path (Fig. 5, supplementary video d & e). The high speed images show that the cavitation bubbles in contact with the biofilm exhibited shape oscillations (or non-spherical shape modes), mostly at mode 3 and mode 4 (Fig. 5). As they contacted the surface, they pierced a hole in the biofilm at the point of contact, then grew as they moved translationally across the surface, disrupting more biofilm in the process (supplementary video f). The radius of the bubbles can also affect the cleaning rate. When the bubbles first contacted the surface, they were small (10–20 µm) but in one case the bubble was larger (100 µm

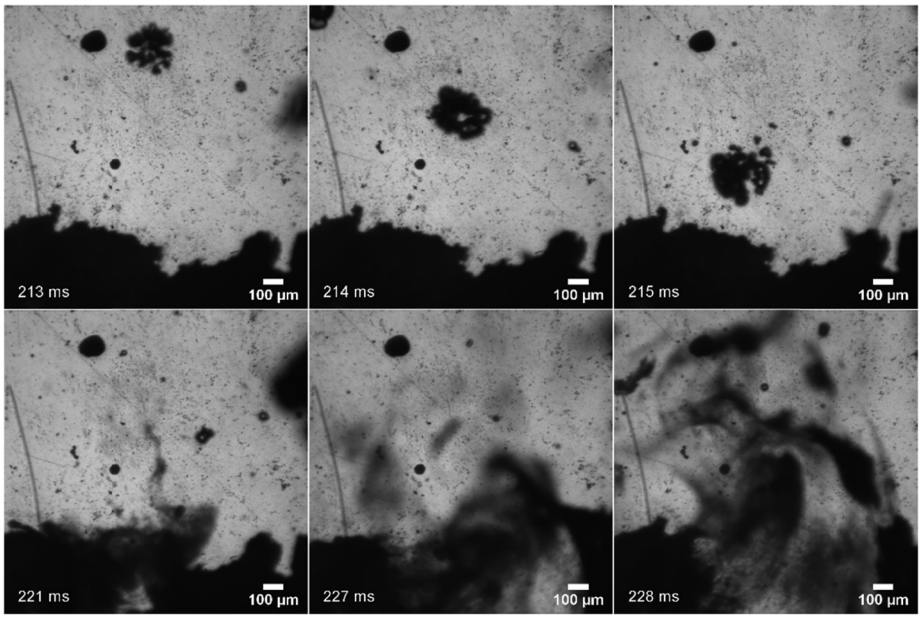

Fig. 4. A cavitating bubble cloud in the water above the surface which then appears to impact the surface just below the field of view, causing biofilm disruption (also see Supplementary video c).

radius) (supplementary video g). Larger bubbles can disrupt a larger area of biofilm, therefore if the bubbles are larger upon contact, this could result in even faster cleaning with cavitation. This could be done by changing parameters affecting cavitation, for example by increasing the gas content of the fluid.

Some channels cleaned by individual oscillating bubbles extend further away from the main area cleaned. Similar extended channels cleaned by cavitation bubbles in patches of a cake layer (fouling occurring in filtration membranes) were observed by Lamminen et al. [10] using scanning electron microscopy. Lamminen et al. speculated this could be due to microstreaming fluid flow, or bubbles travelling along the surface. Based on the real-time imaging results which demonstrate bubbles travelling along the surface, we propose that the results obtained by Lamminen et al. were also due to bubbles travelling across the surface of the cake layer.

Similar bubble behaviour was observed by Reuter et al. [26] where they explain that the bubble is held to the surface via the secondary Bjerknes force and moves across the surface erratically via self-propelling forces, which result from its non-spherical oscillation driven by the pressure wave. Once cavitation bubbles were at a certain distance away from the scaler (approximately 4 mm measured from high speed images), they stopped moving forward on the surface and therefore

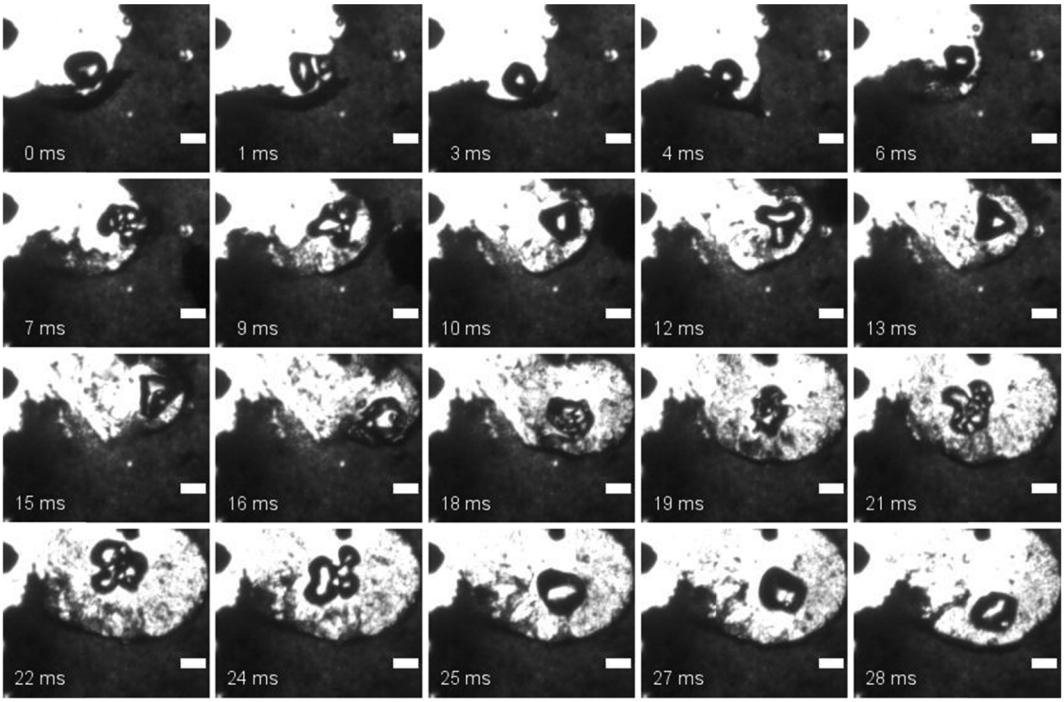

Fig. 5. An individual cavitation bubble forming shape modes, oscillating and disrupting biofilm as it moved across the surface. High speed video available in supplementary video d. Scale bar: 100 µm.

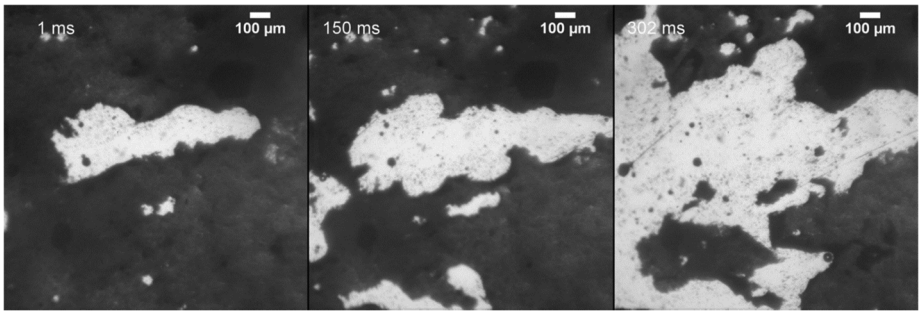

Fig. 6. Biofilm being removed by acoustic streaming, also see supplementary video h.

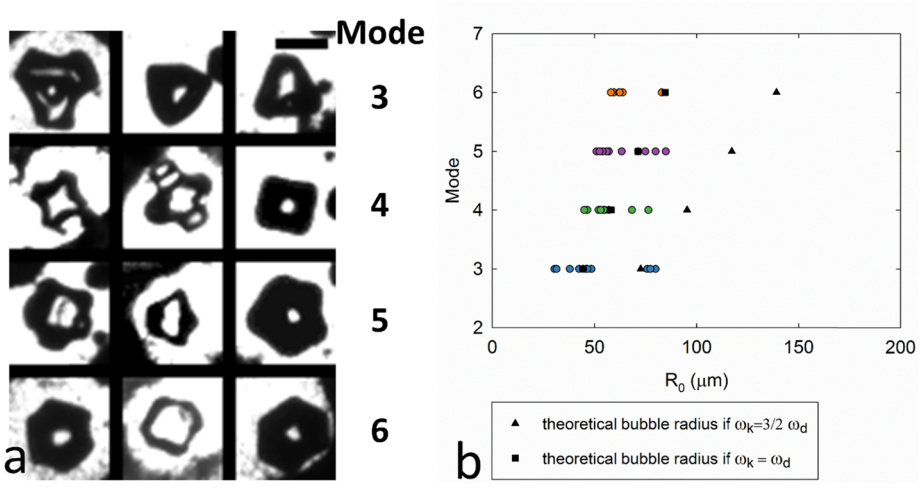

Fig. 7. (a) various bubble shape modes observed for modes 3–6 (b) experimentally observed bubble radius when in different shape modes (coloured symbols) vs the resonant bubble radius at 29 kHz according to Eq. (1).

stopped cleaning. This is likely to be because the acoustic pressure decreases exponentially with distance from the ultrasonic scaler tip.

Individual bubbles appeared to travel underneath the translucent part of the biofilm without disrupting the biofilm surface and emerged out of the biofilm at another location (start of supplementary video b). Reuter et al. [26] also observed a cavitating bubble cleaning a cake layer, which went underneath the surface contaminant to dislodge it from the surface, and it appears that the cavitation bubbles clean in a similar manner when disrupting bacterial biofilm.

The bubbles disrupted the structure of the biofilm first, making it weaker, and then the fluid flow (acoustic streaming) was able to subsequently remove the majority of the biofilm (Fig. 6, supplementary video h). Therefore, for more effective cleaning, it could be useful to use a pressurised water flow after applying the cavitation to remove biofilm quicker once its structure has been weakened by bubbles oscillating on the surface.

Although we have not tested different ultrasonic scalers in this study, it is likely that they will also cause a similar pattern of biofilm disruption. Previous work has used high speed imaging to detect similar cavitation patterns around different shaped ultrasonic scaler tips and also endodontic files [16,23]. The amount of cavitation is related to the vibration amplitude of the scaler tip. The power setting used in this study results in a vibration amplitude of approximately 80 µm, which is in the middle range of vibration amplitudes observed in a previous study [23]. Therefore we anticipate that faster or slower cleaning would occur when using scaler tips with more or less vibration respectively, but since similar cavitation dynamics have been observed around different tips, we anticipate that the method of cleaning will be the same.

3.2. Individual bubble tracking results

Since the experimental images showed that individual bubbles on the surface contributed to biofilm cleaning, we did further image analysis to understand more about these bubbles. We tracked the bubble movements across the surface and calculated their velocity and radius over time. A bubble driven by ultrasound can become shape-unstable through a parametric instability. This triggers particular shape modes corresponding to zonal harmonics of the initially spherical bubble. The shear stress generated by the shape modes at the surface is large and responsible for cleaning. The radii of bubbles oscillating in various shape modes were measured from the high speed images and compared to the theoretical radius of bubbles in resonance. For a gas bubble, the natural angular frequency of shape modes is [27]:

$$\omega_k = \sqrt{(k-1)(k+1)(k+2)\frac{\gamma}{\rho R_{eq}^3}}, \quad (1)$$

where k is the order of the shape mode, γ is the surface tension (0.072 N/m for pure water), ρ is the liquid density (1000 kg/m^3 for water), and R_{eq} is the equilibrium bubble radius. Resonance of shape modes is prone to occur when Mathieu's criterion $2\omega_k/\omega_d = n$ is satisfied, where ω_d is the angular frequency of the acoustic wave and n is a natural number [28]. The frequency of the ultrasonic scaler used in the experiment $f_d = \omega_d/(2\pi)$ was 29,000 kHz. These were plotted against the experimentally observed bubble radii for bubbles in different shape oscillation modes (Fig. 7a), for $\omega_k = \omega_d$ and $\omega_k = 3/2\omega_d$. The occurrence of shape modes is not necessary to satisfy Mathieu's equation. A similar phenomenon was observed by Prabowo & Ohl (2011) [29], where various shape modes of a bubble occurred simultaneously when subject to an acoustic wave. The shape modes that occurred here are likely to have been activated by the translation of bubbles, which is able to induce oscillations of all shape modes as concluded from the perturbation analysis by Doinikov et al. [30].

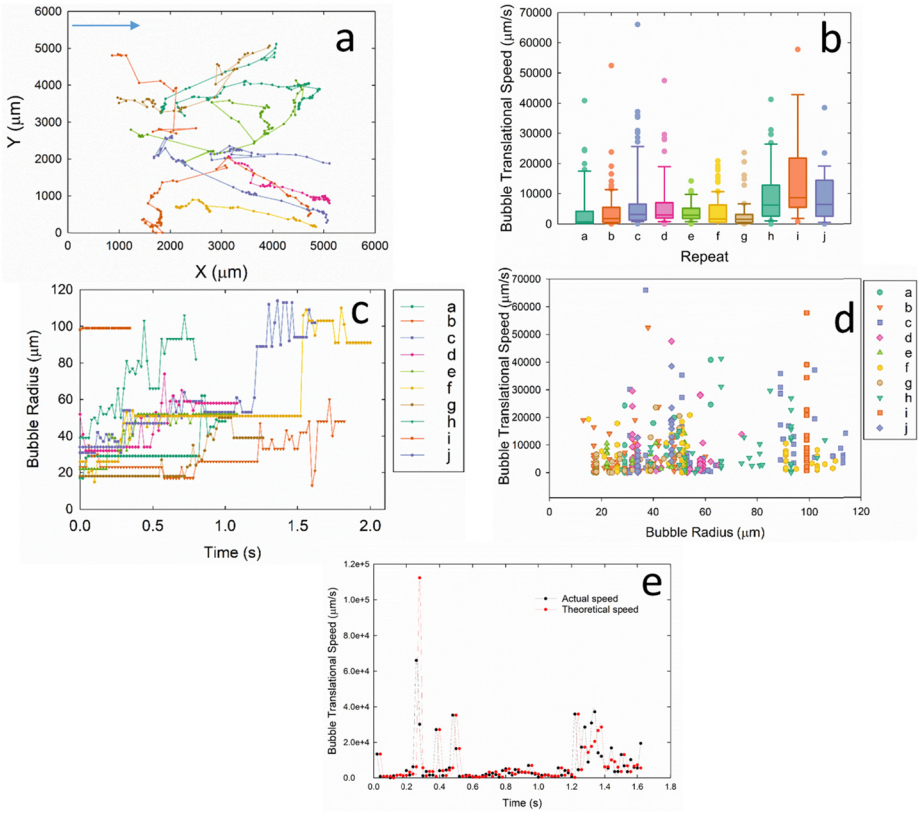

Fig. 8. Bubble tracking results of individual cavitation bubbles disrupting biofilm as they moved across the surface: (a) Tracks generated of bubbles moving across the biofilm, combined from 5 high speed movies. The blue arrow shows the general direction of the bubbles in the video (b) The velocity spread of the bubbles in each of the 10 bubbles tracked from various high speed videos. Each of the tracked bubbles are labelled a to j (c) bubble radius increases over time for all except one tracked bubble, (d) Scatter plot of bubble radius compared to its speed on the surface showing no correlation (e) bubble speed over time for a single track (repeat c in figure b), in comparison to the theoretical speed obtained from Eq. (2). The theoretical speed correlates with the experimental data. (For interpretation of the references to colour in this figure legend, the reader is referred to the web version of this article.)

The growth rate of a bubble in a liquid by rectified diffusion depends on the amplitude and frequency of acoustic waves. In the present cases, the pressure wave is driven by the dental scaler tip displacement. The pressure amplitude around the free end is largest where the displacement amplitude is largest [23]. The bubble growth rate can be estimated by theoretical calculations provided that the gas concentration, driving pressure, and acoustic frequency are known [31,32]. At an acoustic pressure-amplitude of 0.2 MPa at 30 kHz, the growth rate ranges from 10 μm/s to several 100 μm/s depending on the initial bubble radius [33]. The numerical simulation [34] showed that the maximum pressure amplitude for the case considered is in the range 0.1 to 1 MPa decreasing away from the free end. The growth rate of bubble radii shown in Fig. 8c is about 200 μm/s, which is consistent with the results [32,33].

Various shape oscillating microbubbles were tracked using image analysis as they moved across the Thermanox™ coverslip surface to understand more about their radius and speed on the surface. Bubble tracks moved radially away from the ultrasonic scaler tip but were erratic (Fig. 8a). The velocity spread of the bubbles moving across the surface was not constant and the highest speed observed was 68 mm/s (Fig. 8b). For three out of the 10 bubbles tracked, their speed on the surface increased with time. However as this did not occur for all situations we conclude that the bubble speed on the surface was not correlated to the time. Also, the distance away from the ultrasonic scaler tip did not affect the bubble speed. Based on the numerical model, the pressure amplitude decreases with the distance away from the ultrasonic scaler tip [34]. Further work is required to understand what parameters affect the bubble speed on the surface.

The bubble radius increased over time for all except one track (Fig. 8c). There was no correlation between the bubble radius and its speed on the surface as it disrupted biofilm. Larger bubbles however did disrupt a larger area of biofilm, suggesting that larger bubbles could clean biofilm faster, compared to smaller bubbles with the same speed. Therefore, further research with microbubbles which are larger than those of the study, and also with bubbles with a higher velocity across the surface are indicated to determine their effect on the biofilm removal.

The translation velocity of a spherical bubble in an infinite fluid with radius R is given as [20]

$$U(t) = U_0 \frac{R_0^3}{R^3(t)}, \tag{2}$$

where $U(t)$, U_0 is the transient and initial translational velocity of the bubble and $R(t)$, R_0 is its transient and initial radii. According to this equation, a spherical bubble would accelerate as it collapses. Fig. 8d shows the time history of the experimental velocity of a bubble, calculated from the experimental high speed images and its theoretical result obtained from Eq. (2). The experimental results in our work are similar to the theoretical results (Fig. 8d). The differences between them are because the bubbles are not in an infinite fluid but oscillating on a surface and also because they are not spherical.

A possible mechanism for the biofilm disruption occurring around the microbubbles is microstreaming fluid flow around the bubbles in shape oscillation and the associated shear stresses. The order of the shear stress may be calculated as follows. To the first order approximation, the velocity field $\boldsymbol{v}$, at the position $\mathbf{r}$ relative to the bubble centroid, introduced by the shape mode k of an axisymmetric bubble is given as [30]:

$$\mathbf{v}(\mathbf{r}, t) = \frac{a_k}{r^{k+2}}((k+1)P_k(\cos\theta)\mathbf{e}_r + \sin\theta P'_k(\cos\theta)\mathbf{e}_\theta) \quad \text{for } k \geqslant 2 \tag{3}$$

in a spherical coordinate system with the origin at the centre of the bubble, the z-axis being the axis of symmetry, where dot over denotes the derivative to time t, $P_k(\cos\theta)$ is the Legendre polynomial and$P'_k(\cos\theta) = dP_k(\cos\theta)/d\theta$ is the associated Legendre polynomial. a_k is

$$a_k(t) = \frac{R^{k+1}}{k+1}(2s_k\dot{R} + \dot{s}_k R), \tag{4}$$

where s_k denotes the amplitude of shape mode k. The orders of magnitude of the two terms in the brackets in Eq. (4) can be estimated as: $s_k\dot{R} = O(R^2\omega)$, $\dot{s}_k R = O(R^2\omega)$, therefore $a_k(t) = O(R^{k+3}\omega)$. The order of magnitude roughly determines how much larger or smaller one object/effect is compared to others.

The shear stress τ due to the shape mode k of a bubble can be estimated from the flow velocity as following:

$$\tau = O\left(\frac{\mu a_k}{r^{k+3}}\right) = O\left(\mu\omega\left(\frac{R}{r}\right)^{k+3}\right) \tag{5}$$

where μ is the viscosity of the fluid. For the case considered here, μ = 0.07 NS/m^2 and $\omega \approx O(100)$ KHz. We have $\tau = O(10^3)$ N/m^2 near the bubble surface. The shear stress decreases rapidly inversely to the distance r. This is consistent with the fact that cleaning of biofilm occurs very near to oscillating bubbles. This can be seen in supplementary video d, where biofilm is only disrupted when the oscillating bubble is very near to it or in contact with it.

The shape oscillating microbubbles coalesced when meeting each other to form larger microbubbles which could disrupt a larger area of biofilm (supplementary video e). Bubbles may have also formed high speed jets as they moved across the surface, creating shear forces on the surface which disrupted the biofilm. In this study bubble jets could not be observed in high resolution due to the low frame rate required for imaging bubble cleaning effects, however in some instances a ring was observed inside a bubble as it was shape oscillating, which may be the formation of a jet. Bubble jetting may also be occurring during cavitation bubble collapse, which could also be the main cause of biofilm disruption [35]. Bubble jets are one of the main mechanisms responsible of cleaning [36]. The strongest cleaning effect was observed for $\gamma \leq 1.1$ and was explained as the jet spreading flow with the inward flow during the collapse [37]. Numerical simulations confirm this scenario [38].

Another possible mechanism for cleaning by an individual oscillating bubble is due to the Laplace pressure associated with surface tension [39]. Due to surface tension, the pressure inside a bubble p_B is larger than the liquid pressure p_L at the bubble surface

$$\Delta p = p_B - p_L = \frac{2\sigma}{R_c}, \tag{6}$$

where σ is the surface tension (0.072 N/m for pure water) and R_c is the transient curvature radius. As the bubble surface is in contact with the biofilm, the extra pressure Δp pushes away the biofilm in contact with the bubble gas. To estimate the order of magnitude of Δp due to surface tension, we assume that the bubble is spherical and the curvature radius is equal to the bubble radius. The mean experimentally measured bubble radius R in the current study was 58 μm, giving $\Delta p = O(10^3)$ N/m^2.

The shape oscillations in this study are not stable but chaotic, where the bubbles collapse and fragment into smaller microbubbles, which suggests that micro-jets may also be forming during collapse. The clinical instrument used to generate the cavitation in this study has a curved shape producing a variation in the pressure along its length. It is difficult to image jetting and fragmenting of individual microbubbles as this requires the location of the cavitation bubble to be precisely controlled. The high speed camera used in the study is limited by its frame rate, therefore further work could be done using an ultra high speed camera to image a bubble jet impacting a biofilm.

Another limitation of this study is that the plastic coverslip in this study will have different acoustic reflectance properties compared to a biomaterial surface such as titanium or enamel. However a transparent surface was chosen in this study to allow high speed imaging at the highest shutter speed available in bright field mode, to freeze the bubble dynamics so the cleaning mechanisms can be elucidated more accurately. The acoustic impedance of the surface may have an influence of the behaviour of the bubbles. The acoustic impedance of the Thermanox coverslips is not known exactly as it is a proprietary material. However it is a polymer similar to cellulose acetate, which has an acoustic impedance of 3.97 [40]. The acoustic impedance of teeth is 17.8 and that of titanium is 27 [41]. Therefore the bubble behaviour may be different on titanium and teeth, which could be imaged using a different experimental setup, for example using laser illumination or strobe lights as more light would be required for high speed imaging of opaque surfaces.

In addition, during clinical use of an ultrasonic scaler, the cavitation would occur in the cooling water drop flowing over the tip. It is difficult to image the cavitation occurring inside this water bead using a high speed camera due to the constraints of the imaging system. The best approach available was by imaging inside a water tank. Further work could be done to image biofilm removal from this cooling water. Additional studies in a confined space can be carried out in glass samples with drilled spaces representing periodontal pockets around a tooth to resemble more realistic clinical conditions. Inside a periodontal pocket there would be a space where the cooling water would pool and change at low flow rates. The ultrasonic scaler is typically operated in a drip by drip irrigation mode where the flow rate is approximately 0.11 ± 0.01 ml/s. Therefore in this case we envision that the cavitation would still occur and the flow rate may help the cavitation bubbles to move across the surface and clean faster. Nevertheless, the results described are useful to understanding the mechanisms of biofilm removal using cavitation, in a similar manner to other methods such as using an ultrasonic bath. It is assumed that the cleaning mechanisms of the cavitation will be similar, so the results presented in this study are still relevant to aid in optimising biofilm cleaning with ultrasound.

Although for imaging optimisation we used a transparent smooth surface, in a previous study we have also used scanning electron microscopy to image a titanium surface after cleaning with cavitation from a scaler, where similar removal was seen on smooth and rough surfaces. We therefore anticipate that cavitation would operate in a similar manner on rough surfaces similar to the sand blasted acid-etched surface, but if the surface is rougher than this, then it is likely that the cavitation bubbles would travel more slowly across the surface as they would be hampered by the surface roughness, therefore the biofilm removal rate would be lower.

Previous work has applied ultrasonic scaler cavitation to Ti surfaces for up to 60 s [42]. In these studies damage to the Ti surface was not observed, therefore the power of the cavitation occurring around commercially available ultrasonic scalers is not enough to damage implant surfaces. Research could be done to see the effect of the cavitation on soft tissue such as the gums, but in current clinical operation the vibrating ultrasonic scaler tip is put into contact with the teeth and gums, which can cause some bleeding. Therefore the non-touch cavitation method is likely to cause less damage to gums compared to the currently used clinical method.

Previous work investigated biofilm removal after applying the ultrasonic scaler for 15–30 s [42–44]. The results from the current study demonstrate that most of the biofilm can be removed within the first 2 s of operation of the ultrasonic scaler, which would be advantageous in a clinical setting where rapid removal is required. However, the settings used in this study were not able to remove the opaque biofilm clusters, therefore future research could be done to establish the cavitation settings required for complete biofilm removal, as well as to understand more about the biofilm adhesion forces in these clusters compared to the rest of the biofilm. Further research is also required in investigating how biofilm is removed from surfaces with different roughness, and if the bacterial species or a multi-species biofilm affects the removal rate using cavitation. Dental diseases such as periodontitis and peri-implantitis result from complex multi-species bacterial biofilms in the mouth, therefore replicating this experiment with a multispecies biofilm model can give more clinically relevant results. Further work can also be done to investigate how other parameters such as power and distance between the scaler tip and the biofilm affect the biofilm

removal. Combining this experimental data with numerical simulations of the acoustic pressure field and flow velocity will enable cavitation to be used more effectively for biofilm debridement from various surfaces. The experimental techniques used in this study can be used for further work to compare other biofilm removal methods such as strong flow over the slides, and another high speed camera can be added to simultaneously image biofilm removal from the side.

4. Conclusions

Based on the results obtained in this study showing that cavitation bubbles in contact with the surface cause biofilm removal, we recommend that ultrasonic scaler tips can be held as close as possible to the surface to be cleaned to allow cavitation clouds from the tip to make more contact with the biofilm surface. The tracking results showed that cavitation bubbles travelled radially out away up to 4 mm away from the tip. Based on this we can recommend that the tip could be moved 1 cm every 1–2 s to clean larger areas of biofilm effectively. Any remaining biofilm clusters can then be removed by using cavitation at a higher acoustic pressure (i.e. higher instrument power or closer distance between the tip and biofilm). Bacterial biofilm is disrupted rapidly by shape oscillating cavitation bubbles. High speed videos also indicate cavitation cloud cleaning and biofilm removal through acoustic streaming. These results demonstrate an important advance in elucidating the cavitation cleaning mechanisms. Cleaning methods using ultrasonic cavitation can be optimised by ensuring maximum contact of the cavitation bubbles with the surface. The results will help to enable more efficient ultrasonic cleaning of biofilms and the protocol developed in this study can be applied to other studies which investigate surface cleaning.

Declaration of Competing Interest

The authors declare that they have no known competing financial interests or personal relationships that could have appeared to influence the work reported in this paper.

Acknowledgements

This research was funded by the Engineering and Physical Sciences Research Council EP/P015743/1.

Appendix A. Supplementary data

Supplementary data to this article can be found online at https://doi.org/10.1016/j.ultsonch.2020.105112.

References

[1] C.E. Brennen, Cavitation and Bubble Dynamics, Cambridge University Press, 2013.
[2] L. Axelsson, A. Holck, I. Rud, D. Samah, P. Tierce, M. Favre, C. Kure, Cleaning of conveyor belt materials using ultrasound in a thin layer of water, J. Food Prot. 76 (2013) 1401–1407.
[3] P.M. Fratamico, B.A. Annous, N.W. Guenther, Biofilms in the Food and Beverage Industries, Elsevier, 2009.
[4] P. Birkin, D. Offin, C. Vian, R. Howlin, J. Dawson, T. Secker, R. Hervé, P. Stoodley, R. Oreffo, C. Keevil, Cold water cleaning of brain proteins, biofilm and bone–-harnessing an ultrasonically activated stream, Phys. Chem. Chem. Phys. 17 (2015) 20574–20579.
[5] B. Verhaagen, D.F. Rivas, Measuring cavitation and its cleaning effect, Ultrason. Sonochem. 29 (2016) 619–628.
[6] G.W. Gale, A.A. Busnaina, Roles of cavitation and acoustic streaming in megasonic cleaning, Part. Sci. Technol. 17 (1999) 229–238.
[7] B. Felver, D.C. King, S.C. Lea, G.J. Price, A. Damien Walmsley, Cavitation occurrence around ultrasonic dental scalers, Ultrason. Sonochem. 16 (2009) 692–697.
[8] T. Bjarnsholt, The role of bacterial biofilms in chronic infections, APMIS 121 (2013) 1–58.
[9] H. Koo, R.N. Allan, R.P. Howlin, P. Stoodley, L. Hall-Stoodley, Targeting microbial biofilms: current and prospective therapeutic strategies, Nat. Rev. Microbiol. 15 (2017) 740.
[10] M.O. Lamminen, H.W. Walker, L.K. Weavers, Mechanisms and factors influencing the ultrasonic cleaning of particle-fouled ceramic membranes, J. Membr. Sci. 237 (2004) 213–223.
[11] N. Vyas, K. Manmi, Q. Wang, A.J. Jadhav, M. Barigou, R.L. Sammons, S.A. Kuehne, A.D. Walmsley, Which parameters affect biofilm removal with acoustic cavitation? A review, Ultrasound Med. Biol. 45 (2019) 1044–1055.
[12] C.-D. Ohl, M. Arora, R. Dijkink, V. Janve, D. Lohse, Surface cleaning from laser-induced cavitation bubbles, App. Phys. Lett. 89 (2006) 074102.
[13] L. van Wijngaarden, Mechanics of collapsing cavitation bubbles, Ultrason. Sonochem. 29 (2016) 524–527.
[14] D.F. Rivas, B. Verhaagen, J.R.T. Seddon, A.G. Zijlstra, L.-M. Jiang, L.W.M. van der Sluis, M. Versluis, D. Lohse, H.J.G.E. Gardeniers, Localized removal of layers of metal, polymer, or biomaterial by ultrasound cavitation bubbles, Biomicrofluidics 6 (2012) 034114.
[15] R.G. Macedo, J.P. Robinson, B. Verhaagen, A.D. Walmsley, M. Versluis, P.R. Cooper, L.W.M. van der Sluis, A novel methodology providing insights into removal of biofilm-mimicking hydrogel from lateral morphological features of the root canal during irrigation procedures, Int. Endod. J. 47 (2014) 1040–1051.
[16] R.G. Macedo, B. Verhaagen, D. Fernandez Rivas, J.G.E. Gardeniers, L.W.M. van der Sluis, P.R. Wesselink, M. Versluis, Sonochemical and high-speed optical characterization of cavitation generated by an ultrasonically oscillating dental file in root canal models, Ultrason. Sonochem. 21 (2014) 324–335.
[17] J. Robinson, R.G. Macedo, B. Verhaagen, M. Versluis, P. Cooper, L. van der Sluis, A. Walmsley, Cleaning lateral morphological features of the root canal: the role of streaming and cavitation, Int. Endod. J. (2017).
[18] S. Dhir, Biofilm and dental implant: the microbial link, J. Indian Soc. Periodontol. 17 (2013) 5.
[19] P. Schmage, F. Kahili, I. Nergiz, T.M. Scorziello, U. Platzer, P. Pfeiffer, Cleaning effectiveness of implant prophylaxis instruments, Int. J. Oral Maxillofac. Implants 29 (2014) 331–337.
[20] J.T. Steigenga, K.F. Al-Shammari, F.H. Nociti, C.E. Misch, H.-L. Wang, Dental implant design and its relationship to long-term implant success, Implant Dent. 12 (2003) 306–317.
[21] J. Pratten, A. Smith, M. Wilson, Response of single species biofilms and microcosm dental plaques to pulsing with chlorhexidine, J. Antimicrob. Chemother. 42 (1998) 453–459.
[22] M. Lodovici, L. Raimondi, F. Guglielmi, S. Gemignani, P. Dolara, Protection against ultraviolet B-induced oxidative DNA damage in rabbit corneal-derived cells (SIRC) by 4-coumaric acid, Toxicology 184 (2003) 141–147.
[23] N. Vyas, E. Pecheva, H. Dehghani, R.L. Sammons, Q.X. Wang, D.M. Leppinen, A.D. Walmsley, High speed imaging of cavitation around dental ultrasonic scaler tips, PLoS ONE 11 (2016) e0149804.
[24] J. Schindelin, I. Arganda-Carreras, E. Frise, V. Kaynig, M. Longair, T. Pietzsch, S. Preibisch, C. Rueden, S. Saalfeld, B. Schmid, J.-Y. Tinevez, D.J. White, V. Hartenstein, K. Eliceiri, P. Tomancak, A. Cardona, Fiji: an open-source platform for biological-image analysis, Nat. Meth. 9 (2012) 676–682.
[25] J.-Y. Tinevez, N. Perry, J. Schindelin, G.M. Hoopes, G.D. Reynolds, E. Laplantine, S.Y. Bednarek, S.L. Shorte, K.W. Eliceiri, TrackMate: an open and extensible platform for single-particle tracking, Methods 115 (2017) 80–90.
[26] F. Reuter, S. Lauterborn, R. Mettin, W. Lauterborn, Membrane cleaning with ultrasonically driven bubbles, Ultrason. Sonochem. 37 (2017) 542–560.
[27] H. Lamb, Hydrodynamics, Cambridge University Press, 1993.
[28] Y. Liu, Q. Wang, Stability and natural frequency of nonspherical mode of an encapsulated microbubble in a viscous liquid, Phys. Fluids 28 (2016) 062102.
[29] F. Prabowo, C.-D. Ohl, Surface oscillation and jetting from surface attached acoustic driven bubbles, Ultrason. Sonochem. 18 (2011) 431–435.
[30] A.A. Doinikov, Translational motion of a bubble undergoing shape oscillations, J. Fl. Mech. 501 (2004) 1–24.
[31] F. Grieser, P.-K. Choi, N. Enomoto, H. Harada, K. Okitsu, K. Yasui, Sonochemistry and the acoustic bubble, Elsevier, 2015.
[32] M.M. Fyrillas, A.J. Szeri, Dissolution or growth of soluble spherical oscillating bubbles: the effect of surfactants, J. Fl. Mech. 289 (1995) 295–314.
[33] L.A. Crum, Measurements of the growth of air bubbles by rectified diffusion, J. Acoust. Soc. Am. 68 (1980) 203–211.
[34] K. Manmi, W. Wu, N. Vyas, W. Smith, Q. Wang, A. Walmsley, Numerical investigation of cavitation generated by an ultrasonic dental scaler tip vibrating in a compressible liquid, Ultrason. Sonochem. 104963 (2020).
[35] R. Bolaños-Jiménez, M. Rossi, D.F. Rivas, C.J. Kähler, A. Marin, Streaming flow by oscillating bubbles: quantitative diagnostics via particle tracking velocimetry, J. Fl. Mech. 820 (2017) 529–548.
[36] G.L. Chahine, A. Kapahi, J.-K. Choi, C.-T. Hsiao, Modeling of surface cleaning by cavitation bubble dynamics and collapse, Ultrason. Sonochem. 29 (2016) 528–549.
[37] F. Reuter, R. Mettin, Mechanisms of single bubble cleaning, Ultrason. Sonochem. 29 (2016) 550–562.
[38] Q. Zeng, S.R. Gonzalez-Avila, R. Dijkink, P. Koukouvinis, M. Gavaises, C.-D. Ohl, Wall shear stress from jetting cavitation bubbles, J. Fl. Mech. 846 (2018) 341–355.
[39] W. Kim, T.-H. Kim, J. Choi, H.-Y. Kim, Mechanism of particle removal by megasonic waves, App. Phys. Lett. 94 (2009) 081908.
[40] J. Lochab, V. Singh, Acoustic behaviour of plastics for medical applications, 2004.
[41] S. Lees, Specific acoustic impedance of enamel and dentine, Arch. Oral Biol. 13 (1968) 1491–1500.
[42] N. Vyas, R.L. Sammons, O. Addison, H. Dehghani, A.D. Walmsley, A quantitative method to measure biofilm removal efficiency from complex biomaterial surfaces using SEM and image analysis, Sci. Rep. 6 (2016) 32694.
[43] T. Thurnheer, E. Rohrer, G.N. Belibasakis, T. Attin, P.R. Schmidlin, Static biofilm removal around ultrasonic tips in vitro, Clin. Oral Investig. 18 (2014) 1779–1784.
[44] S.J. Gartenmann, T. Thurnheer, T. Attin, P.R. Schmidlin, Influence of ultrasonic tip distance and orientation on biofilm removal, Clin. Oral Invest. 21 (2017) 1029–1036.